Characterization of dynamic regulation in Chinese Hamster Ovary (CHO) cell cultures

Sha Sha[1], Bingyu Kuang[2], Seongkyu Yoon[1,2 *]

[1] Biomedical Engineering and Biotechnology, University of Massachusetts Lowell, Lowell, MA 01854, USA

[2] Chemical Engineering, University of Massachusetts Lowell, Lowell, MA 01854, USA

[*] Corresponding Author:

Seongkyu Yoon (Seongkyu_Yoon@uml.edu)

1 University Ave, Lowell MA 01854

Phone: 978-934-4741

Fax: 978-934-3047

Abstract

Chinese hamster ovary (CHO) cells are the most used host cells in the biopharmaceutical industry for the production of biologics medicine. During batch or fed-batch processes that are commonly used, cells undergo an exponential growth phase where a high percentage of cells remain rapid growth. However, the culture environment such as media condition keep varying during this process. The responses of cells to culture environment change during a batch of culture remain implicit. Despite extensive studies in literature on cellular transition from exponential to stationary phase, there is a lack of study on cell regulations at the exponential growth phase, commonly assuming the exponential phase as a "steady-state" phase. This study generated RNA-seq data from the transcriptome of three CHO cell lines across the exponential growth phase. The result explains the dynamic pattern of the gene expressions for glycolysis, TCA, glycosylation and anti-oxidant enzyme genes, gaining insights of transcriptomic level regulation. It was also observed with a series of genes gathered around 91st hour that a micro-environment is having a concurrent shift. The time point was coincident with lactate shift from accumulation to consumption. The gene expressions altogether suggest a homeostasis behavior prior to 91st hour, as possibly a response to the high abundance of nutrient at the early exponential growth phase.

1 Introduction

As the main workhorse in the biopharmaceutical industry, Chinese hamster ovary (CHO) cells are used for producing a variety of biologics including monoclonal antibodies (mAbs). Cells are commonly cultured in the process modes of batch and fed-batch. In these circumstances, cells need to experience dynamic changes in the culture environment which is constituted by nutrient depletion, cell density increase, byproduct accumulation and so on. A full understanding of cellular behavior during the dynamic course of culture remains implicit. One set of important tools to gain more understanding is through omics approaches.

The insights of cellular metabolism in cultures have been increased from the last decade. As a layer of regulation prior to other post-transcription stage, transcriptomic data underline many cellular activities and are commonly studied [1-3]. During the various stages across cell culture, the cellular regulations across the exponential to stationary phase of culture have been intensively studied [4-8]. Exponential phase is the period when cell density rapidly increase. Nevertheless, the duration of exponential phase has been less studied. A pseudo-steady state has been commonly assumed, and the insights of gene expression dynamics within this phase were in general overlooked.

Interactions are found to be present among many pathways in cellular processes, such as the association found among apoptosis, lactate and pyruvate metabolism [9]; glycosylation and oxidative potential [10], oxidative stress and glycolysis, nucleotide sugar synthesis and sialylation [11] and so on. However, as discussions were conventionally focused on specified activities of cells, one shortage is viewing the holistic pictures of transient microenvironment in cells. This can be improved by the usage of RNA-seq technology. Lately, RNA-seq has been increasingly applied to examine global environment of CHO cells [12-14]. It also becomes

amenable to obtain a comprehensive evaluation of cellular metabolism by the diverse pathways that can be covered by RNA-seq data.

In this study, global gene expression in batch culture was profiled using RNA-seq technology. A focus was made to reveal the transcriptomic regulations over the exponential phases. Three cell lines were used in the study to draw consensus results across cell lines. The study examined the dynamic gene expression at the central metabolism, N-linked glycosylation and the redox environment. From the data, a shift of transcriptome at 91 h in the culture was found with genes from various pathways. A picture of a homeostatic effort of cells during the exponential phase is thus formed from those observations.

2 Results

2.1 Cell culture

The culture of three cell lines A, B and R were conducted in triplicate flasks and lasted 150 h. As shown in **Fig. 1**, all the culture remained more than 90% viability before 140 h. A decline of cell line A growth started around 103 h while the other two cell lines remained their growth rates. The transcriptomic differentiation regarding the growth and titer production was discussed in our previous study [13], while this study would focus on the dynamic behavior of the three cell lines across the exponential phase. Metabolically, the glucose was constantly consumed and the depletion occurred around 120 h. The glutamine remained at a low level near the instrument's detection limit. At 91 h, lactate shifted from accumulation to consumption. The ammonia and glutamate trends were fluctuating throughout the culture. The pH varied within a range of 7.2 and 7.6 with the early decrease concurrent with the lactate accumulation, and a later increase with the lactate consumption.

The study considered 60 to 130 h to be a general exponential phase from the three cell lines. The behavior of the biological replicates within this period was consistent, as seen by the small error bars among the triplicate culture. Cell mRNAs were extracted and sequenced at five time points: 67, 91, 117, 121 and 127 h. The period of time points being sequenced is shaded in Fig.1.

2.2 Clusters of time-series global transcriptome

As the first step of investigating into the transcriptome, the global transcriptomic data from the five time points were imported in a principal component analysis (PCA). Data of replicate culture were included. The analyses were used to cluster the time points according to the similarity of the states of transcriptome.

The data from each cell line were first individually analyzed (**Fig.2A to 2C**). In Fig.2B and Fig.2C, the early and late time points (except 91 h) in the case of B and R were clustered. A dynamic trend moves overall from the bottom to the top in the plots as time progresses, however, one cluster was overall formed blending the late time and early time points. In contrast, cell line A (Fig.2A) had made a clear distinction between the last time point (127 h) and the earlier time points, forming two clusters. The gene ontology (GO) enriched from the differentially expressed genes between 121 and 127 h in cell line A (altered greater than 1.4 folds, p-adj<0.01) indicates a negative regulation of maintenance of mitotic sister chromatid cohesion. Cell line B and R came up without any GO functions enriched during this period.

Notably, a distinct cluster of transcriptome was found at 91 h for all the three cell lines (highlighted with the yellow circle in **Fig.2A-2C**). This unique cluster indicates that a transcriptomic shift occurred from 67 h to 91 h, followed by a shift back to the previous status after 91 h. Accordingly, genes directing this feature should have a shifted regulation across 91 h,

which would be further explored by examining gene expressions in the specific pathways in the following results.

To verify the findings from the individual cell line, the PCA was conducted with data comprising all the three cell lines (Fig.2D). The analysis confirmed that the distinction found at the latest stage of cell line A and the distinct status at 91 h were both present with the data combining all the three cell lines.

2.3 Landscape of gene expression

Before investigating the genes from metabolic pathways, a landscape of the expression levels was first gained of the genes at different pathways considered in this study. The gene expression levels at 67 h (the first time point sequenced) are plotted in **Fig.3**. The full names of genes are listed in **Table S1**. The results show that the levels of the gene expression were consistent among the three cell lines. The energy associated central metabolism including glycolysis and TCA had generally high expressions of genes. Several genes in the glycolysis show superior expression abundance; those genes are *Ldha*, *Pgk1*, *Gapdh*, *Pkm*, *Aldoa*, *Pgam1* and *Tpi1*.The anti-oxidant enzyme genes also had substantial expression. Relatively, the glycosylation pathway genes overall had lower expression.

2.4 Time-course gene expression in energy pathways

The dynamic expressions of genes from Glycolysis and TCA pathways, as well as a metabolic network are shown in **Fig. 4**. The full names of metabolites in the network are listed in **Table S2**. The results included a total of 22 expressed glycolytic genes/isoforms and 25 expressed TCA genes/isoforms. The genes are labeled numerically in the network, data plots and Table S1. Data at each time point are normalized to the expression at 67 h.

The dynamic changes of the genes are found to be mostly smaller than 2 folds. Most of the highly-expressing glycolytic genes shown in Fig.3 had constant decrease in expression. A series of other genes also showed decreasing expression. Among those genes, *Pkm* encodes an isoform of pyruvate kinase (*Pkm*) that expresses a rate-limiting enzyme of glycolysis reactions. There are only a small number of genes that showed increase during exponential phase, including the glucose intake transporter Glut1 *(Slc2a)*. Notably, a number of glycolytic genes were found to increase before 91 h and decrease after, forming a shift in trend surrounding 91 h. These genes are summarized in **Table 1** along with the genes from other pathways that showed the same shift.

Like glycolytic genes, most of the genes from TCA showed decreasing trend, initiated either at 67 h (the first time point) or 91 h (the second time point). A small number of genes showed increase, including the genes *glul*, which encodes glutamine synthetase that catalyzes the synthesis of glutamine; this gene was also highly expressed (600-1000 tpm). The gene *gls* which encodes glutaminase that degrades glutamine into glutamate and ammonium was minimally expressed (<30 tpm). The extracellular metabolic profiles indicate that ammonia was consumed while glutamate was flat during the investigated period, suggesting a possible stage that ammonia and glutamate were used to synthesize glutamine. The increasing and abundant expression of *Glul* and the subtle expression of *Gls* matched such phenotype.

Pyruvate is an important node in the transition of glycolytic and TCA fluxes, thus the branches of pyruvate distribution and the genes associated with in-fluxes and out-fluxes of pyruvate are pulled out and shown in **Fig. S1**. It was found that the *Pkm* (producing pyruvate from glycolysis) decreased and the *Pck2* (producing pyruvate from TCA) increased overtime, suggesting a reduced flow from glycolysis but an increased replenish to pyruvate from TCA. The increase of *Pck2* after 91 h was substantial (greater than 2 time folds) for cell line B. In the

meantime, an anaplerotic gene *Pc* increased prior to 91 h, indicating the support to TCA from glycolysis.

2.5 Time-course gene expression in glycosylation pathways

Fifty-four glycosylation genes from literature [4] were analyzed from the RNA-seq data. These genes participate in the glycosylation at the steps of nucleotide sugar synthesis, nucleotide sugar transport, glycan extension, galactosylation, sialylation, fucosylation and degradation. Among those, forty-three genes were found expressed. The dynamic expressions of the genes after normalization are shown in **Fig.5**, and mostly showed mild changes (< 2 folds) over time. However, a number of genes showed a shift at 91 h, and the degree of the shift was nearly as large as two folds. These genes were found from almost every step in the glycosylation process and are also summarized in **Table 1**. Another group of genes found with significant variation dynamically was the group of glycosidases. Except Neuraminidase 3 (*Neu3*), the glycosidases were found increasing during the investigated period, including fucosidase (*Fuca1*), hexosaminidase subunit alpha (*Hexa*), galactosidase Beta 1 (*glb1*) and neuraminidase 1 (*Neu1*).

2.6 Genes associated with redox environment

To view the gene expression in the redox environment, three major enzymes in the anti-oxidative enzyme systems, including Glutathione peroxidase (*Gpx*), superoxide dismutase (*Sod*) and gene catalase (*Cat*) were first examined and the dynamic trends are shown in **Fig.6**.

The gene *Gpx1*, one of the most important antioxidant enzymes that protect cells from damage by oxidative stress, showed a decreasing trend overtime. Another gene Selenoprotein W 1(*Sepw1*) encodes a selenoprotein of redox function, was found to have similar decreasing expression over time. Notably, the genes of *Gpx1* and *Sepw1* were the genes of the largest change found in the transcriptome by folds more than two folds (p-adj <0.01) over 24 h. The

Sod1, one isoform gene of *Sod*, showed the same trend as the *Gpx1* gene. The regulatory gene *p53* which plays a role in anti-oxidative stress activity associated with glutathione peroxidase was also found with a decreasing trend.

Another two anti-oxidative genes, the *Sod2* (another isoform gene of *Sod)* and *Cat* (the other anti-oxidant enzyme) showed a shift at 91 h. In the meantime, several other genes associated with redox environment were found to have the same shift at 91 h. These genes include: (1) *Hif1α,* which is a main unit of hypoxia-inducible factor, a transcriptional factor ubiquitously expressed responding to oxidative stress. (2) *Pdk3*, an isoform of pyruvate dehydrogenase kinase which inhibits pyruvate dehydrogenase to enhance glycolytic and inhibits TCA pathways. (3) *G6pd,* encoding glucose-6-phosphate dehydrogenase which is the enzyme converting G6P to pentose phosphate pathway (PPP). (4) *Casp3,* which encodes Caspase 3 and responsible for apoptosis regulation.

2.7 qRT-PCR confirmation of mRNA data

To examine the reliability of RNA-seq data, qRT-PCR was used to validate several genes **(Fig.7)**. Three genes of glycosidase (*Fuca, Hexa* and *Glb1*) and one gene associated with oxidative stress (*Gpx1*) were chosen to be tested due to their apparent trends showed over the course. A pair of biological replicates A1 and A2 were included in the tests. As the result, *Pgx1*, *Fuca*, *Hexa* showed tight consistency with RNA-seq. The only discrepancy occurred was *Glb1* which showed a decreasing trend at the last two time points from qRT-PCR; while in the RNA-seq data the expression of *Glb1* showed increase throughout the entire culture.

3 Discussion

3.1 Insights on dynamic expressions of central metabolism, glycosylation and redox genes

192 Via the investigation of the three cell lines, the dynamic changes of gene expression at the
193 central metabolism and glycosylation pathways were in general smaller than 2-folds. This
194 indicates that the change in the transcriptome during the exponential phase is milder compared to
195 the changes observed cross exponential and stationary phases [1]. The gene expression dynamics
196 were in majority similar among the three cell lines over the pathways of glycolysis, TCA and
197 glycosylation. However, a unique transition was seen for the cell line that underwent declining
198 stage in the case of cell line A. The transcriptomic variation during the transition was associated
199 with DNA replication.

200 The dynamic behaviors of genes in glycolysis and TCA match many understandings
201 currently existing from the metabolic point of view [15, 16]. This includes larger glycolytic flux
202 than TCA fluxes in CHO cells, known as the "Warburg Effect" [17]. Consistently found in this
203 study, several glycolytic genes were expressed significantly higher than the rest of glycolytic
204 genes and TCA genes; coincidently, these genes showed decrease prolonging the exponential
205 phase. The dynamic trends of glycolytic and TCA genes are diverse, nevertheless, most genes
206 including one encoding a limiting enzyme showed decreasing expression over the course, overall
207 in agreement with other studies that showed decrease of metabolic fluxes over culture [18, 19].
208 Finally, the trends of the genes surrounding pyruvate indicate a support to increase fluxes to
209 TCA cycle as culture progresses. This is in agreement with the understanding from a previous
210 flux study that showed a transition from glycolysis to TCA metabolism over culture [20].

211 From glycosylation pathways, the group of glycosidase enzymes catalyzing the degradation
212 of glycan was surprisingly found increasing during the early exponential phase. It was previously
213 known that glycosidase increase at stationary phase typically since ammonia accumulation forms
214 a possible inducer of glycosidase enzymes [7]. The increasing expression of glycosidase at the

early stage of exponential phase may attract necessary attention in the culture process in the concern of glycosylation profile [6].

In the redox system, enzymes in the anti-oxidant system are responsible for different roles and maintained under balance [21]. Among the genes examined in this study, *Gpx1* and *Sod1* showed similarly decreasing trends while *Sod2* and *Cat* showed a different trend. The decrease of *Gpx1* expression could be further correlated with two other decreasing genes: *Sepw1* and *p53*. Specifically, the genes *Sepw1* encodes a selenoprotein and plays a role in redox-related process. *Sepw1* not only showed similar trends as *Gpx1*, but the two genes were decreased with similarly large magnitudes (more than 2 folds). The regulatory gene *p53* was known to play a role in both apoptosis and anti-oxidative stress activity and be associated with Gpx [22]; the consensus p53 binding sequence was identified in human *Gpx* promoter regions [23]. The possible co-regulation between the *P53* and *Gpx1* found in this study was in line with this understanding.

3.2 Regulatory microenvironment at 91 h

A micro-environment was shown at 91 h indicating a transition of cellular status. A key feature of this micro-environment is the concurrent shift of the expression trends from the genes (as summarized in **Table 1**) from various pathways. These genes underline the distinct transcriptomic status at 91 h found in the first glance of the PCA result. A homeostatic effort associated with redox environment was suggested by this study and summarized in **Fig.8**.

Redox balancing is an important part of homeostasis; its role is to avoid reactive oxygen species (ROS) accumulation [24]. In this study, the shift of genes *Sod2* and *Cat* encoding anti-oxidant enzymes before and after 91 h indicate a presence of redox regulation. This regulation

has triggered other associated regulation. This included *Hif1α*, an important transcriptional factor that regulates cellular adaption in response to oxidative stress [15].

As a consequence of *Hif1* regulation: The shift also occurred with *Pdk*, the gene encoding pyruvate dehydrogenase kinase that enhances glycolysis and inhibits TCA; this effort could be present in order to mitigate ROS production in mitochondria [15, 25]. Another gene got regulated was the *G6pd*, which expresses glucose-6-phosphate dehydrogenase, the rate-limiting enzyme for converting glycolysis to oxidative PPP. It was known that G6pd could be controlled by the NADPH redox status [22], and that the NADPH produced in PPP pathway not only supports nucleic acid synthesis but also regulates the homeostasis of oxidative stress [26].

Besides *Pdk* and *G6pd*, several glycolytic and TCA genes were also found to have a shifting trend at 91 h, as summarized in Table 1. Even though these changes were at a small degree, they could contribute to the regulation associated with the redox environment. In addition, apoptosis and autophagy could be triggered under stress according to literature [27]; in this study, this regulation was exemplified by the shift found with *Casp3*, the gene encoding caspase 3.

It was previously reported that glycosylation is affected at the hypoxic regulation [28]. In our results, a number of genes from glycosylation pathways showed co-occurred regulation at 91 h. These genes are involved in synthesizing glycan precursors (especially with mannose, N-acetylglucosame and galactose), as well as transporting these precursors from cytoplasm to Golgi and modification on glycan. Interestingly, several studies in literature have shown shifting trends in the intracellular nucleotide sugar profiles during cell culture [29-31].

Finally, the redox regulation might have also been associated with the lactate shift which was concurrently found in the culture. Lactate shift is a common phenomenon in cell culture. Recent

studies revealed many insights behind lactate shift. For example, studies identified different metabolic states before and after lactate shifts [18-20]. Lactate shift has also been linked with AKT1 signaling pathways that involve a series of genes regulating glycolysis and redox environment [32, 33]. Consistently in this study, a series of transcriptomic co-events found at apoptosis, hypoxia and oxidative stress in this study were well in agreement with the phenomenon reported at lactate shift occurrence in literature [25, 34-36]. We also proposed that lactate shift could be triggered by the redox microenvironment. As shown in **Fig.8**, before 91 h, the redox regulation stimulated protective regulation by promoting glycolysis; under which circumstance the lactate was produced. After 91 h, oxidative stress decreased and TCA was promoted. This transition triggered the start of the consumption of lactate.

The onset of redox-associated regulation is not clear, but one plausible reason can be the high abundance of nutrient at the start of culture. It was reported that excess nutrients can cause excessive mitochondria oxidative metabolism, consequentially arising oxidative stress [37]. CHO cells take excess glucose at the start of the culture at the abundance of glucose, and mitochondria is a main place of oxidative metabolism and ROS production. A short-term regulation was likely present in cells to mitigate the upcoming stress in TCA with the aid of anti-oxidative enzymes and upregulating glycolysis. Correspondingly, the decrease in such regulation afterward could be due to the decrease of glucose and the pressure on TCA activity after 91 h.

To conclude, the homeostatic effort summarized above suggests a redox-triggered regulation and its associated microenvironment. This regulation activity shows that during the steady growth of cells in the exponential phase, regulations as needed can be made by cells for adjusting microenvironment to maintain intracellular homeostasis.

4 Methods

4.1 Cell culture

The three GS-CHO cell lines used in this study were donated by industrial collaborators. Cells were parented from CHO-S and engineered to respectively produce Adalimumab, Bevacizumab and Rituximab biosimilars (each cell line was respectively called A, B and R in the study). Cells were thawed and proceeded in a seed culture until reaching the exponential phase. Cells were then inoculated at a density of 0.3 million per ml in 250 mL shake flasks with 50 mL working volume. Each cell line was cultured with triplicate flasks and a batch mode at 37 ºC, 5% CO_2 and 125 rpm incubator. CD-FortiCHO media (ThermoFisher Scienrific, Waltham, MA) was used for all the culture without glutamine supplementation.

4.2 Cell culture analysis

Cells were counted by Cedex Hires Analyzer (Roche Life Science, Indianapolis, IN). Basic metabolites including glucose, lactate, ammonia and glutamate were measured using NovaProfile analyzer (Nova Biomedical, Waltham, MA). Mab titer was measured by Waters Alliance 2695 high-performance liquid chromatography system (HPLC) (Waters, Milford, MA) in alliance with POROS® A 20 µm column (Thermo Fisher Scientific, Waltham, MA).

4.3 RNA extraction

Approximately 5 million cells were stored in RLT buffer (Qiagen, Germantown, MD) and saved at -80 ºC. The total RNAs were extracted using RNeasy mini kit (Qiagen, Valencia, CA) following the manufactures' instructions and quantified using Qubit Florometer (ThermoFisher Scientific, Waltham, MA). Integrity values of the extracted RNAs were examined by Bioanalyzer (Agilent technologies, Santa Clara, CA).

4.4 RNA-seq and data processing

The mRNAs were extracted from total RNA and converted to cDNA with dual indexes using Illumina mRNA stranded library preparation kit (Illumina, San Diego, CA). The cDNA libraries were loaded onto the high output flow cells and sequenced by NextSeq 500 (Illumina, San Diego, CA). The fastq data were uploaded to Massachusetts Green High Performance Computing Center (GHPCC) and processed via Dolphin, an online data analysis interface developed by UMass medical school (https://dolphin.umassmed.edu/). The analysis pipeline started from data quality check to aligning the short reads to a reference database. The details of the pipeline could be found in a previous publication [13]. The RSEM produces two types of counts in the result: estimated counts (non-normalized) and the normalized values of transcript per million reads (tpm). These two formats of data were respectively used in the differential gene analysis and the dynamic profiles of gene expression.

4.5 Transcriptomic data analyses

Principal component analysis (PCA) and differential expression gene (DEG) analysis were performed using the built-in tools in Debrowser [38]. Genes with the most varied 1000 genes were used as inputs in the PCA. DEG analysis was conducted by DESeq2 using the expected counts from RSEM as inputs. A threshold of p-adj < 0.01 (Benjamini-Hochberg process) was applied in the significance of analysis. The expression data of genes associated with particular pathways were extracted from the gene expression results by assistance of an R-based Bioconductor “mygene” package. The normalized data in transcripts per million reads (tpm) were used to analyze the dynamic trends of gene expressions. GO functions of gene sets were conducted using a web-based tool Gorilla [39].

4.6 Quantitative reverse transcription PCR (qRT-PCR)

RNAs were converted to cDNA using the SS3 superscript kit (Invitrogen, Carlsbad, CA) following the manufactures' instructions. The cDNAs were diluted twenty times and quantified using 7500 Real Time PCR System (ThermoFisher Scientific, Waltham, MA). The *Gapdh* was chosen as an internal control gene. The primers of the four genes tested and the *Gapdh* are listed in the **Table S3**. The PCR was run with the following program: 50°C for 2 min; 95°C for 10 min, 40-50 cycles at 59°C for 1 min, 55-60°C for 20s, and 95°C for 15s. The transcript level was represented by the expression level normalized to *Gapdh* in logarithm scale.

Acknowledgement

The study was supported by NSF/MRI (1428272) and NSF/IUCRC AMBIC (1624718). The authors gratefully thank Dr. Maurizio Cattaneo for providing the cell-lines, and Jack Lepine from UMass Lowell Core Research Facility (CRF) and two graduate students, Zhuangrong Huang and Seo-young Park from Dr. Yoon's group for their participation in the work.

Author Contributions

Sha S. designed and conducted the RNA-seq experiments and analyses. Kuang B. conducted the verification of RNA-seq results by qRT-PCR. Yoon S. was the PI of the project and provided main supervision and guidance to the research work. All the authors reviewed and approved the manuscript. The authors declare that they have no competing financial interests.

Reference

1. Bort, J.A.H., et al., *Dynamic mRNA and miRNA profiling of CHO-K1 suspension cell cultures.* Biotechnology Journal, 2012. **7**(4): p. 500-15.
2. Korke, R., et al., *Large scale gene expression profiling of metabolic shift of mammalian cells in culture.* Journal of Biotechnology, 2004. **107**(1): p. 1-17.
3. Le, H., et al., *Dynamic gene expression for metabolic engineering of mammalian cells in culture.* Metab Eng, 2013. **20**: p. 212-20.
4. Lee, J.H., et al., *Understanding of decreased sialylation of Fc-fusion protein in hyperosmotic recombinant Chinese hamster ovary cell culture: N-glycosylation gene expression and N-linked glycan antennary profile.* Biotechnol Bioeng, 2017.
5. Lee, S.M., et al., *Digital mRNA profiling of N-glycosylation gene expression in recombinant Chinese hamster ovary cells treated with sodium butyrate.* J Biotechnol, 2014. **171**: p. 56-60.
6. Sha, S., et al., *N-Glycosylation Design and Control of Therapeutic Monoclonal Antibodies.* Trends in Biotechnology, 2016. **34**(10): p. 835-846.
7. Ha, T.K., Y.G. Kim, and G.M. Lee, *Understanding of altered N-glycosylation-related gene expression in recombinant Chinese hamster ovary cells subjected to elevated ammonium concentration by digital mRNA counting.* Biotechnol Bioeng, 2015. **112**(8): p. 1583-1593.
8. Rodrigo, M.-A. and D.A. J., *Multiplexed digital mRNA expression analysis profiles system-wide changes in mRNA abundance and responsiveness of UPR-specific gene expression changes during batch culture of recombinant Chinese Hamster Ovary cells.* 2018, 2018.
9. Templeton, N., et al., *The impact of anti-apoptotic gene Bcl-2 expression on CHO central metabolism.* Metab Eng, 2014. **25**: p. 92-102.
10. Dionne, B., N. Mishra, and M. Butler, *A low redox potential affects monoclonal antibody assembly and glycosylation in cell culture.* J Biotechnol, 2017. **246**: p. 71-80.
11. Lewis, A.M., et al., *Understanding and Controlling Sialylation in a CHO Fc-Fusion Process.* PLoS One, 2016. **11**(6): p. e0157111.
12. Orellana, C.A., et al., *RNA-Seq highlights high clonal variation in monoclonal antibody producing CHO cells.* Biotechnology Journal, 2017.
13. Sha, S., H. Bhatia, and S. Yoon, *An RNA-seq based transcriptomic investigation into the productivity and growth variants with Chinese Hamster Ovary cells.* J Biotechnol, 2018.
14. Hsu, H.H., et al., *A Systematic Approach to Time-series Metabolite Profiling and RNA-seq Analysis of Chinese Hamster Ovary Cell Culture.* Sci Rep, 2017. **7**: p. 43518.
15. Mulukutla, B.C., et al., *Regulation of Glucose Metabolism - A Perspective From Cell Bioprocessing.* Trends Biotechnol, 2016. **34**(8): p. 638-51.
16. Mulukutla, B.C., et al., *Multiplicity of steady states in glycolysis and shift of metabolic state in cultured mammalian cells.* PLoS One, 2015. **10**(3): p. e0121561.
17. Mulukutla, B.C., et al., *Glucose metabolism in mammalian cell culture: new insights for tweaking vintage pathways.* Trends Biotechnol, 2010. **28**(9): p. 476-84.
18. Ahn, W.S. and M.R. Antoniewicz, *Metabolic flux analysis of CHO cells at growth and non-growth phases using isotopic tracers and mass spectrometry.* Metab Eng, 2011. **13**(5): p. 598-609.
19. Selvarasu, S., et al., *Combined data preprocessing and multivariate statistical analysis characterizes fed-batch culture of mouse hybridoma cells for rational medium design.* J Biotechnol, 2010. **150**(1): p. 94-100.
20. Selvarasu, S., et al., *Elucidation of metabolism in hybridoma cells grown in fed-batch culture by genome-scale modeling.* Biotechnol Bioeng, 2009. **102**(5): p. 1494-1504.
21. Trachootham, D., et al., *Redox regulation of cell survival.* Antioxid Redox Signal, 2008. **10**(8): p. 1343-74.

22. Ahn, W.S. and M.R. Antoniewicz, *Towards dynamic metabolic flux analysis in CHO cell cultures.* Biotechnol J, 2012. **7**(1): p. 61-74.
23. Sablina, A.A., et al., *The antioxidant function of the p53 tumor suppressor.* Nat Med, 2005. **11**(12): p. 1306-13.
24. Gao, Y., et al., *Combined metabolomics and proteomics reveals hypoxia as a cause of lower productivity on scale-up to a 5000-liter CHO bioprocess.* Biotechnol J, 2016. **11**(9): p. 1190-1200.
25. Brand, K., *Aerobic Glycolysis by Proliferating Cells: Protection against Oxidative Stress at the Expense of Energy Yield.* Journal of Bioenergetics and Biomembrane, 1997. **29**(4).
26. Sengupta, N., S.T. Rose, and J.A. Morgan, *Metabolic flux analysis of CHO cell metabolism in the late non-growth phase.* Biotechnol Bioeng, 2011. **108**(1): p. 82-92.
27. Hussain, S.P., et al., *p53-Induced Up-Regulation of MnSOD and GPx but not Catalase Increases Oxidative Stress and Apoptosis.* Cancer research, 2004.
28. Shirato, K., et al., *Hypoxic regulation of glycosylation via the N acetylglucosamine cycle.* J. Clin. Biochem. Nutr. , 2011. **48**(1): p. 20-25.
29. Kochanowski, N., et al., *Intracellular nucleotide and nucleotide sugar contents of cultured CHO cells determined by a fast, sensitive, and high-resolution ion-pair RP-HPLC.* Anal Biochem, 2006. **348**(2): p. 243-51.
30. Villiger, T.K., et al., *High-throughput profiling of nucleotides and nucleotide sugars to evaluate their impact on antibody N-glycosylation.* J Biotechnol, 2016. **229**: p. 3-12.
31. Jedrzejewski, P.M., et al., *Towards controlling the glycoform: a model framework linking extracellular metabolites to antibody glycosylation.* Int J Mol Sci, 2014. **15**(3): p. 4492-4522.
32. Mulukutla, B.C., M. Gramer, and W.S. Hu, *On metabolic shift to lactate consumption in fed-batch culture of mammalian cells.* Metab Eng, 2012. **14**(2): p. 138-49.
33. Hartley, F., et al., *Mechanisms Driving the Lactate Switch in Chinese Hamster Ovary cells.* Biotechnology and Bioengineering, 2017.
34. Zagari, F., et al., *Lactate metabolism shift in CHO cell culture: the role of mitochondrial oxidative activity.* N Biotechnol, 2013. **30**(2): p. 238-45.
35. Sauerwald, T.M., et al., *Combining caspase and mitochondrial dysfunction inhibitors of apoptosis to limit cell death in mammalian cell cultures.* Biotechnol Bioeng, 2006. **94**(2): p. 362-72.
36. Dorai, H., et al., *Expression of anti-apoptosis genes alters lactate metabolism of Chinese Hamster Ovary cells in culture.* Biotechnol Bioeng, 2009. **103**(3): p. 592-608.
37. Wellen, K.E. and C.B. Thompson, *Cellular metabolic stress: considering how cells respond to nutrient excess.* Mol Cell, 2010. **40**(2): p. 323-32.
38. Kucukural, A., N. Merowsky, and M. Garber, *Debrowser: debrowser: Interactive Differential Expresion Analysis Browser. R package version 1.2.4.* https://github.com/UMMS-Biocore/debrowser, 2016.
39. Eden, E., et al., *GOrilla: a tool for discovery and visualization of enriched GO terms in ranked gene lists.* BMC Bioinformatics, 2009. **10**(48): p. 1-7.

Tables

Table 1: Genes shifting expression at 91 h

Genes	Function
Glycolysis	
Gpi	Glucose-6-phosphate isomerase
Pgm1	Phosphoglucomutase 1
Pfkm	Phosphofructokinase, muscle
Bpgm	Bisphosphoglycerate Mutase
Hk1	Hexokinase 1
Minpp1	2,3-Bisphosphoglycerate 3-Phosphatase
Pfkp	Phosphofructokinase, platelet
TCA	
Cs	Citrate synthase
Idh1	Isocitrate dehydrogenase
Oghd	Oxoglutarate (alpha-ketoglutarate) dehydrogenase-like
Pc	Pyruvate carboxylase
Gls	Glutaminase
Glycosylation synthesis	
Ugp2	UDP-Glucose pyrophosphorylase; G1P+UTP - > UDP-Glc
Dpm1	Dolichyl-phosphate mannosyltransferase subunit 1
Mannose trimming	
Manea	Mannosidase endo-alpha
Man1c1	Mannosyl-oligosaccharide 1,2-alpha-mannosidase
Nucleotide sugar transport	
Slc35a1	CMP-sialic acid transporter
Slc35d2	UDP-GlcNAc/UDP-Glucose transporter
Galactosylation	
B4galt1	Beta-1,4-Galactosyltransferase 1
B4gat5	Beta-1,4-Galactosyltransferase 5
Sialylation	
St3gal1	ST3 Beta-Galactoside Alpha-2,3-Sialyltransferase 1
St3gal6	ST3 Beta-Galactoside Alpha-2,3-Sialyltransferase 6
Fucosylation	
Fut8	Fucosyltransferase 8
Oxidative regulation	
Hif1a	Hypoxia induced factor 1a
Pdk3	Pyruvate dehydrogenase kinase
Casp3	Caspase-3
G6pd	Glucose-6-phosphate dehydrogenase
SOD2	Superoxide dismutase 1, soluble, Mn dependent, in mitocondria
Cat	Catalase, transcript variant X1

Figure Legends

Figure 1 Cell growth, titer production, metabolites and pH profiles of a batch culture of three cell lines A, B and R. The error bars shown in data indicate the variation from the three replicate cultures.

Figure 2 Principal component analysis (PCA) of time-series transcript data. The patterns of time-series transcriptome from (A) cell line A; (B) cell line B, (C) cell line R and (D) combination of cell line A, B and R. The clusters are indicated by circles. The yellow circle indicates a distinct transcriptomic status at 91 h.

Figure 3 Gene expression at 67 h (first time point sequenced) from the pathways of glycolysis, TCA, redox related environment and the steps in glycosylation including nucleotide sugar synthesis, nucleotide sugar transport, N-glycan extension, galactosylation, sialylation and glycosidase activity. The error bars shown in data indicate the variation from the three replicate cultures.

Figure 4 A central metabolism network and gene expression level. (A) A network of glycolysis, TCA and pentose phosphate pathways. The full names of genes and metabolites are given in Table S1 - S2. (B) Time series expression of genes at glycolysis. (C) Time-series expression of genes at TCA. The genes at glycolysis sand TCA pathways were categorized into four groups of trends (i) decreasing; (ii) increasing followed by decreasing (a shift); (iii) increasing; (iv) no clear trends.

Figure 5 Dynamic expression of glycosylation pathway genes. (A) Genes of nucleotide sugar synthesis; (B) Nucleotide sugar transport; (C) N-glycan extension; (D) Galactosylation; (E) Sialylation; (F) Fucosylation; (G) Glycosidases.

Figure 6 Redox related genes. (A) Expression of anti-oxidative genes; (B) Redox-related genes.

Figure 7 Comparison of RNA-seq and RT-PCR results with four selected genes.

Figure 8 An overview of gene regulation in a hemostatic microenvironment before and after 91 h.

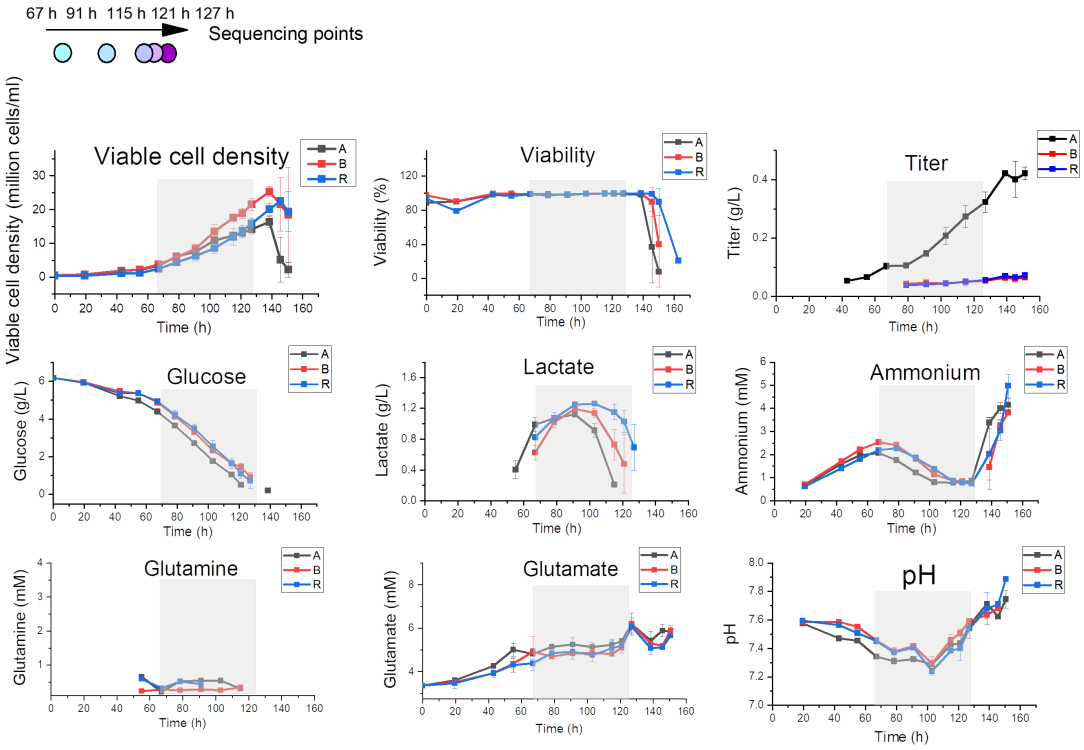
67 h 91 h 115 h 121 h 127 h
Sequencing points
Viable cell density
Viable cell density (million cells/ml)
Viability
Viability (%)
Titer
Titer (g/L)
Glucose
Glucose (g/L)
Lactate
Lactate (g/L)
Ammonium
Ammonium (mM)
Glutamine
Glutamine (mM)
Glutamate
Glutamate (mM)
pH
Time (h)
A
B
R

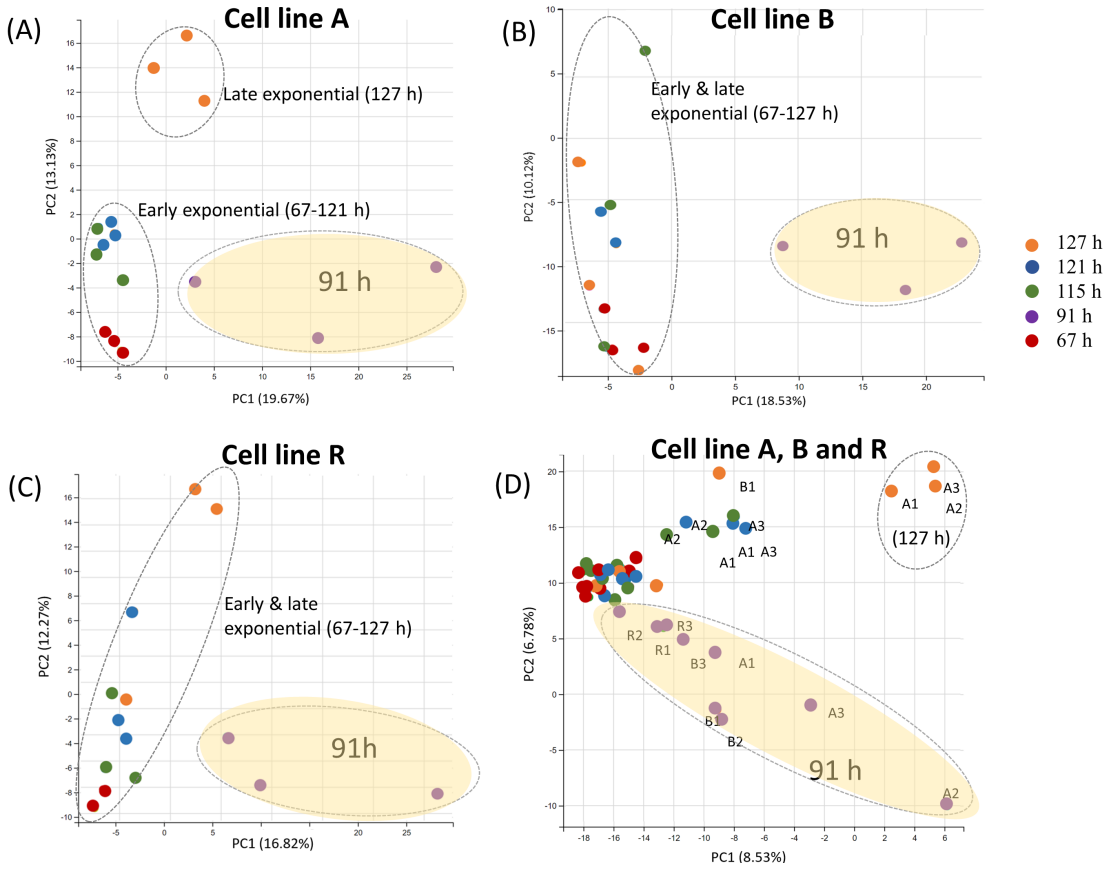
(A)
Cell line A
Late exponential (127 h)
Early exponential (67-121 h)
91 h
PC2 (13.13%)
PC1 (19.67%)
(B)
Cell line B
Early & late
exponential (67-127 h)
91 h
PC2 (10.12%)
PC1 (18.53%)
127 h
121 h
115 h
91 h
67 h
(C)
Cell line R
Early & late
exponential (67-127 h)
91h
PC2 (12.27%)
PC1 (16.82%)
(D)
Cell line A, B and R
(127 h)
91 h
PC2 (6.78%)
PC1 (8.53%)

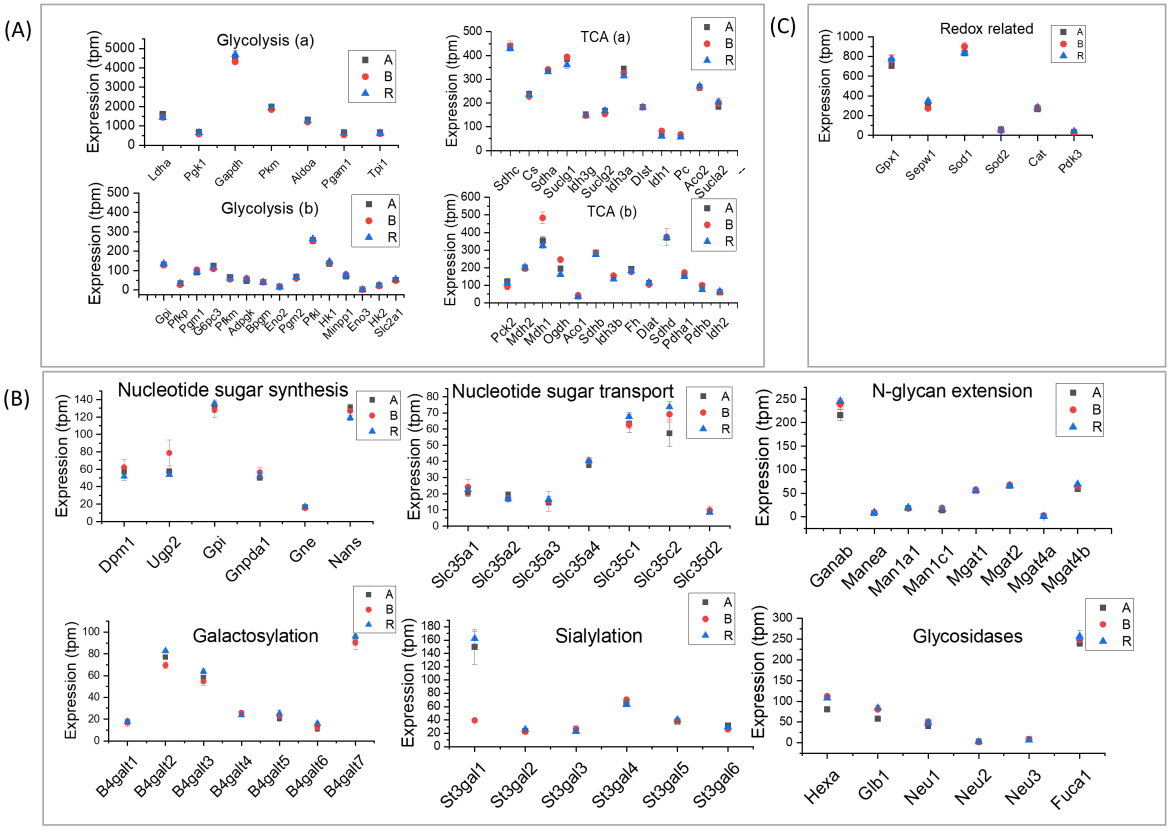
(A)
Glycolysis (a)
Expression (tpm)
A
B
R
Ldha
Pgk1
Gapdh
Pkm
Aldoa
Pgam1
Tpi1
TCA (a)
Sdhc
Cs
Sdha
Suclg1
Idh3g
Suclg2
Idh3a
Dlst
Idh1
Pc
Aco2
Sucla2
Glycolysis (b)
Gpi
Pfkp
Pgm1
Gapdh
Pkm
Aldpgk
Bpgm
Eno2
Pgm2
Pfkl
Hk1
Mmgp1
Eno3
Hk2
Slc2a1
TCA (b)
Pck2
Mdh2
Mdh1
Ogdh
Aco1
Sdhb
Idh3b
Fh
Dlat
Sdhd
Pdha1
Pdhb
Idh2
(C)
Redox related
Gpx1
Sepw1
Sod1
Sod2
Cat
Pdk3
(B)
Nucleotide sugar synthesis
Dpm1
Ugp2
Gpi
Gnpda1
Gne
Nans
Nucleotide sugar transport
Slc35a1
Slc35a2
Slc35a3
Slc35a4
Slc35c1
Slc35c2
Slc35d2
N-glycan extension
Ganab
Manea
Man1a1
Man1c1
Mgat1
Mgat2
Mgat4a
Mgat4b
Galactosylation
B4galt1
B4galt2
B4galt3
B4galt4
B4galt5
B4galt6
B4galt7
Sialylation
St3gal1
St3gal2
St3gal3
St3gal4
St3gal5
St3gal6
Glycosidases
Hexa
Glb1
Neu1
Neu2
Neu3
Fuca1

(A)

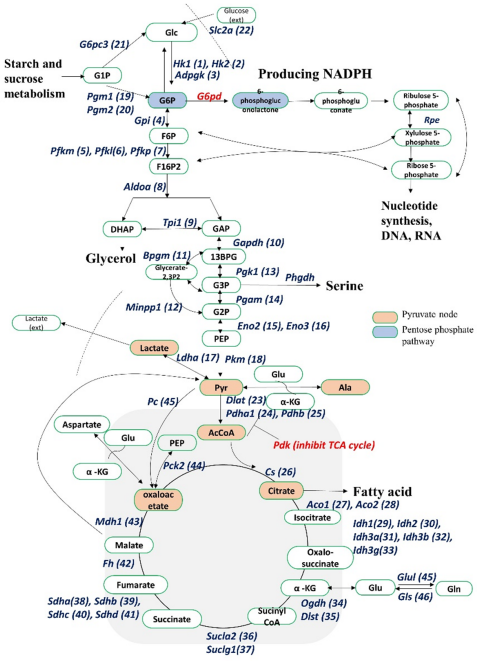
Starch and sucrose metabolism
G1P
G6pc3 (21)
Glc
Glucose (ext)
Slc2a (22)
Hk1 (1), Hk2 (2)
Adpgk (3)
Producing NADPH
Pgm1 (19)
Pgm2 (20)
G6P
G6pd
phosphoglucono lactone
phosphogluconate
Ribulose 5-phosphate
Rpe
Xylulose 5-phosphate
Ribose 5-phosphate
Gpi (4)
F6P
Pfkm (5), Pfkl(6), Pfkp (7)
F16P2
Aldoa (8)
Nucleotide synthesis, DNA, RNA
DHAP
Tpi1 (9)
GAP
Gapdh (10)
Glycerol
Bpgm (11)
13BPG
Glycerate-2,3P2
Pgk1 (13)
Phgdh
G3P
Serine
Pgam (14)
Minpp1 (12)
G2P
Eno2 (15), Eno3 (16)
PEP
Lactate (ext)
Lactate
Ldha (17)
Pkm (18)
Pyruvate node
Pentose phosphate pathway
Glu
Pyr
Ala
Dlat (23)
α-KG
Pdha1 (24), Pdhb (25)
Pc (45)
Aspartate
Glu
PEP
AcCoA
Pdk (inhibit TCA cycle)
α -KG
Pck2 (44)
Cs (26)
Citrate
Fatty acid
oxaloacetate
Aco1 (27), Aco2 (28)
Isocitrate
Idh1(29), Idh2 (30), Idh3a(31), Idh3b (32), Idh3g(33)
Mdh1 (43)
Malate
Oxalo-succinate
Fh (42)
Fumarate
α -KG
Glu
Glul (45)
Gls (46)
Gln
Sdha(38), Sdhb (39), Sdhc (40), Sdhd (41)
Succinate
Succinyl CoA
Ogdh (34)
Dlst (35)
Sucla2 (36)
Suclg1(37)

(B)

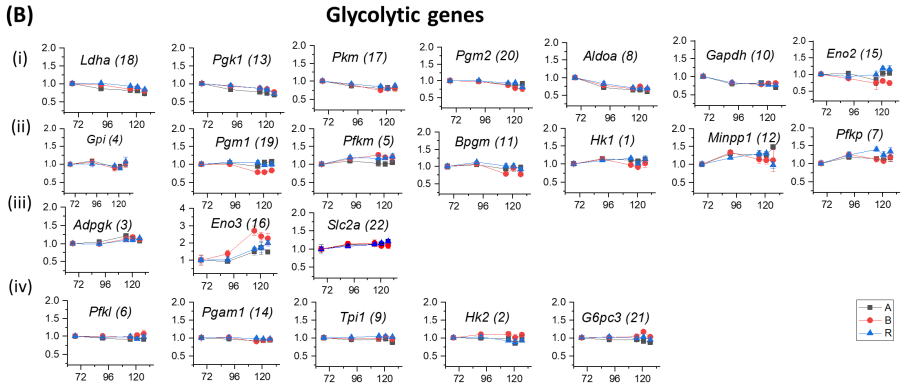
Glycolytic genes
(i)
Ldha (18)
Pgk1 (13)
Pkm (17)
Pgm2 (20)
Aldoa (8)
Gapdh (10)
Eno2 (15)
(ii)
Gpi (4)
Pgm1 (19)
Pfkm (5)
Bpgm (11)
Hk1 (1)
Minpp1 (12)
Pfkp (7)
(iii)
Adpgk (3)
Eno3 (16)
Slc2a (22)
(iv)
Pfkl (6)
Pgam1 (14)
Tpi1 (9)
Hk2 (2)
G6pc3 (21)
A
B
R

(C)

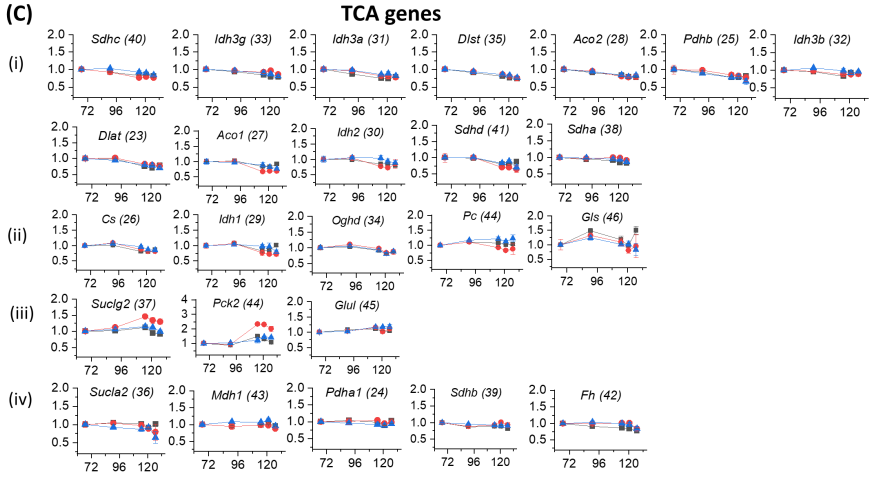
TCA genes
(i)
Sdhc (40)
Idh3g (33)
Idh3a (31)
Dlst (35)
Aco2 (28)
Pdhb (25)
Idh3b (32)
Dlat (23)
Aco1 (27)
Idh2 (30)
Sdhd (41)
Sdha (38)
(ii)
Cs (26)
Idh1 (29)
Oghd (34)
Pc (44)
Gls (46)
(iii)
Suclg2 (37)
Pck2 (44)
Glul (45)
(iv)
Sucla2 (36)
Mdh1 (43)
Pdha1 (24)
Sdhb (39)
Fh (42)

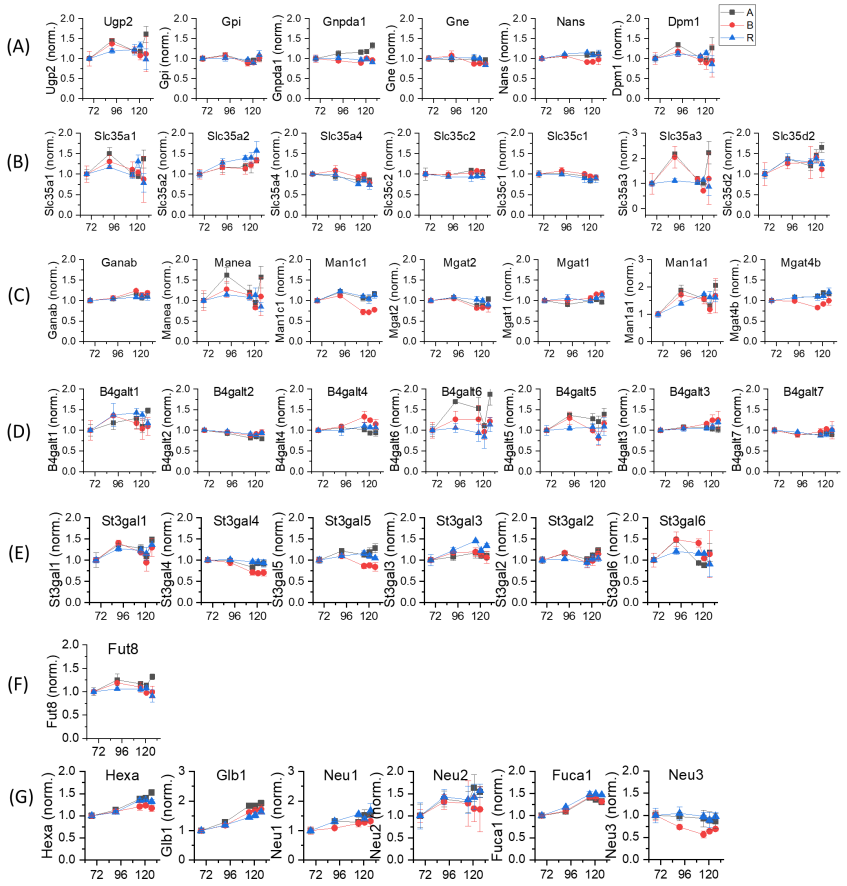
(A)
Ugp2
Gpi
Gnpda1
Gne
Nans
Dpm1
A
B
R
(B)
Slc35a1
Slc35a2
Slc35a4
Slc35c2
Slc35c1
Slc35a3
Slc35d2
(C)
Ganab
Manea
Man1c1
Mgat2
Mgat1
Man1a1
Mgat4b
(D)
B4galt1
B4galt2
B4galt4
B4galt6
B4galt5
B4galt3
B4galt7
(E)
St3gal1
St3gal4
St3gal5
St3gal3
St3gal2
St3gal6
(F)
Fut8
(G)
Hexa
Glb1
Neu1
Neu2
Fuca1
Neu3
72 96 120

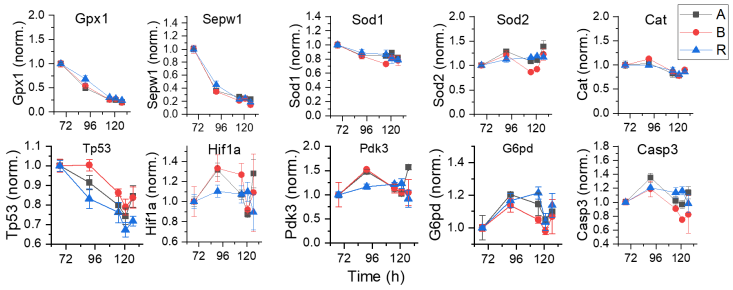
Gpx1
Sepw1
Sod1
Sod2
Cat
Tp53
Hif1a
Pdk3
G6pd
Casp3
Gpx1 (norm.)
Sepw1 (norm.)
Sod1 (norm.)
Sod2 (norm.)
Cat (norm.)
Tp53 (norm.)
Hif1a (norm.)
Pdk3 (norm.)
G6pd (norm.)
Casp3 (norm.)
Time (h)
A
B
R

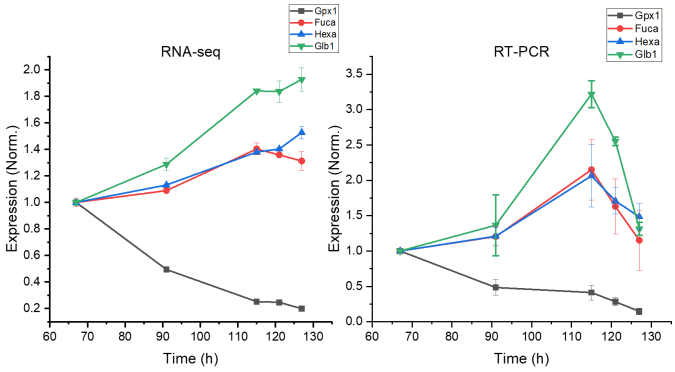
RNA-seq
RT-PCR
Gpx1
Fuca
Hexa
Glb1
Expression (Norm.)
Time (h)
60
70
80
90
100
110
120
130
0.2
0.4
0.6
0.8
1.0
1.2
1.4
1.6
1.8
2.0
0.0
0.5
1.0
1.5
2.0
2.5
3.0
3.5

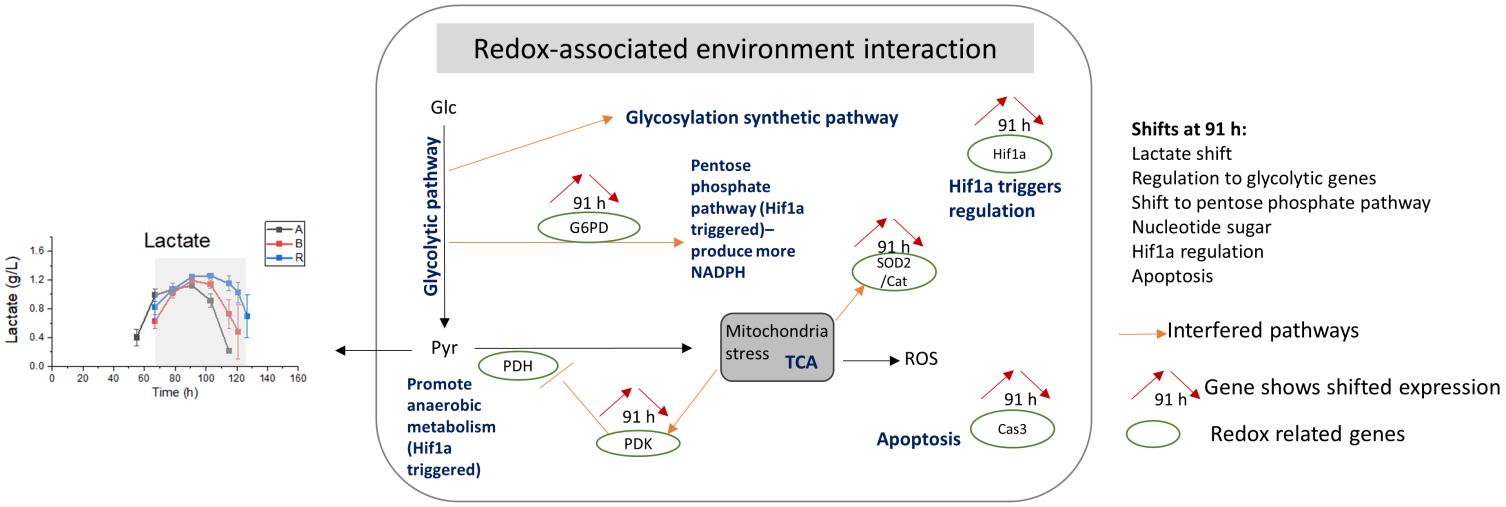
Lactate
A
B
R
Lactate (g/L)
Time (h)
Redox-associated environment interaction
Glc
Glycosylation synthetic pathway
91 h
Hif1a
Hif1a triggers regulation
Glycolytic pathway
91 h
G6PD
Pentose phosphate pathway (Hif1a triggered)– produce more NADPH
91 h
SOD2 /Cat
Pyr
PDH
Mitochondria stress
TCA
ROS
Promote anaerobic metabolism (Hif1a triggered)
91 h
PDK
91 h
Cas3
Apoptosis
Shifts at 91 h:
Lactate shift
Regulation to glycolytic genes
Shift to pentose phosphate pathway
Nucleotide sugar
Hif1a regulation
Apoptosis
Interfered pathways
91 h
Gene shows shifted expression
Redox related genes